Supplementary Material

Catalytic partitioning and divergent steroidogenic effects of CYP17A1 inhibition by seviteronel and abiraterone

Jibira Yakubu[1,2,3], Therina du Toit[2, 4], Kodzo Atchou[5], Shripriya Singh[1,2], Anna Matveeva[1,2,3], Flemming Steen Jørgensen[6] , Amit V. Pandey[1,2,7*]

[1]Pediatric Endocrinology, Diabetology, and Metabolism, University Children's Hospital, Inselspital, Bern, Switzerland.

[2]Translational Hormone Research Program, Department of Biomedical Research, Faculty of Medicine, University of Bern, Bern, Switzerland.

[3]Graduate School for Cellular and Biomedical Sciences, University of Bern, Bern, Switzerland.

[4]Department of Nephrology and Hypertension, University Hospital Bern, Inselspital, 3010 Bern, Switzerland.

[5]Institute for Cell Biology, University of Bern, Switzerland.

[6]Department of Drug Design and Pharmacology, University of Copenhagen, DK-2100 Copenhagen, Denmark

[7]Department of Digital Medicine, University of Bern, 3008 Bern, Switzerland

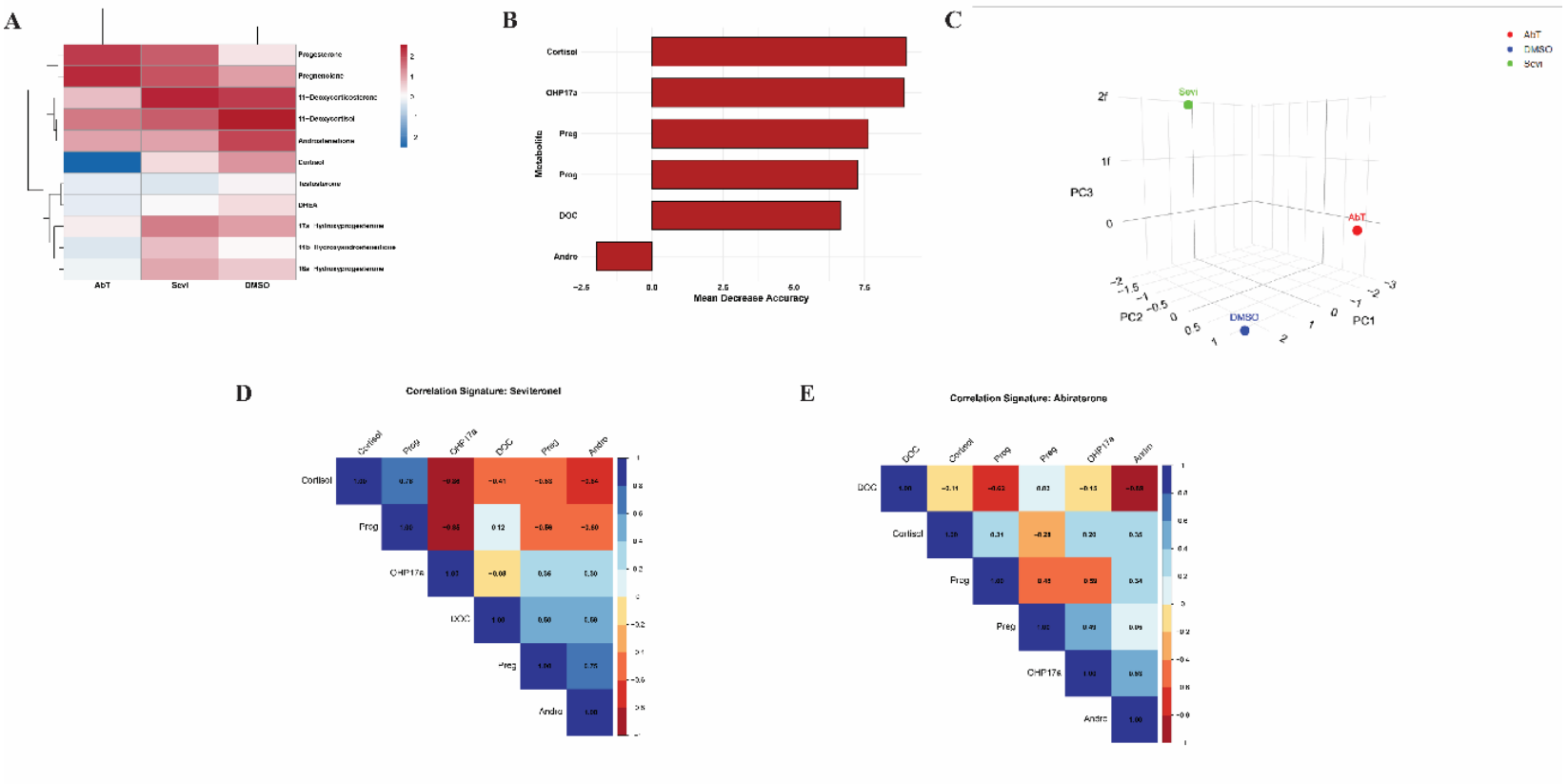

Figure S1. Exploratory multivariate analysis identifies distinct treatment-associated steroid profiles. (A) Hierarchical clustering heatmap of log10-transformed steroid concentrations following treatment with vehicle (DMSO), abiraterone (AbT), or seviteronel (Sevi). Abiraterone treatment is characterized by marked accumulation of upstream precursors and depletion of several downstream steroid products, whereas seviteronel produces a distinct profile with greater preservation of selected 17α-hydroxylated and mineralocorticoid-pathway intermediates. **(B)** Random Forest variable-importance analysis showing the metabolites contributing most strongly to treatment-group discrimination in this dataset; DOC and 17α-hydroxyprogesterone (17OHP) are among the highest-ranking features. **(C)** Three-dimensional principal-component analysis (PCA) showing separation of the three treatment-associated steroid profiles in the projected PCA space; PC1 accounts for >80% of the observed variance. **(D,E)** Pearson correlation matrices for seviteronel (**D**) and abiraterone (**E**) treatment groups. The negative association between DOC and androstenedione under seviteronel is consistent with altered partitioning between mineralocorticoid and androgen pathways, whereas abiraterone shows strong positive associations among accumulated upstream precursors.

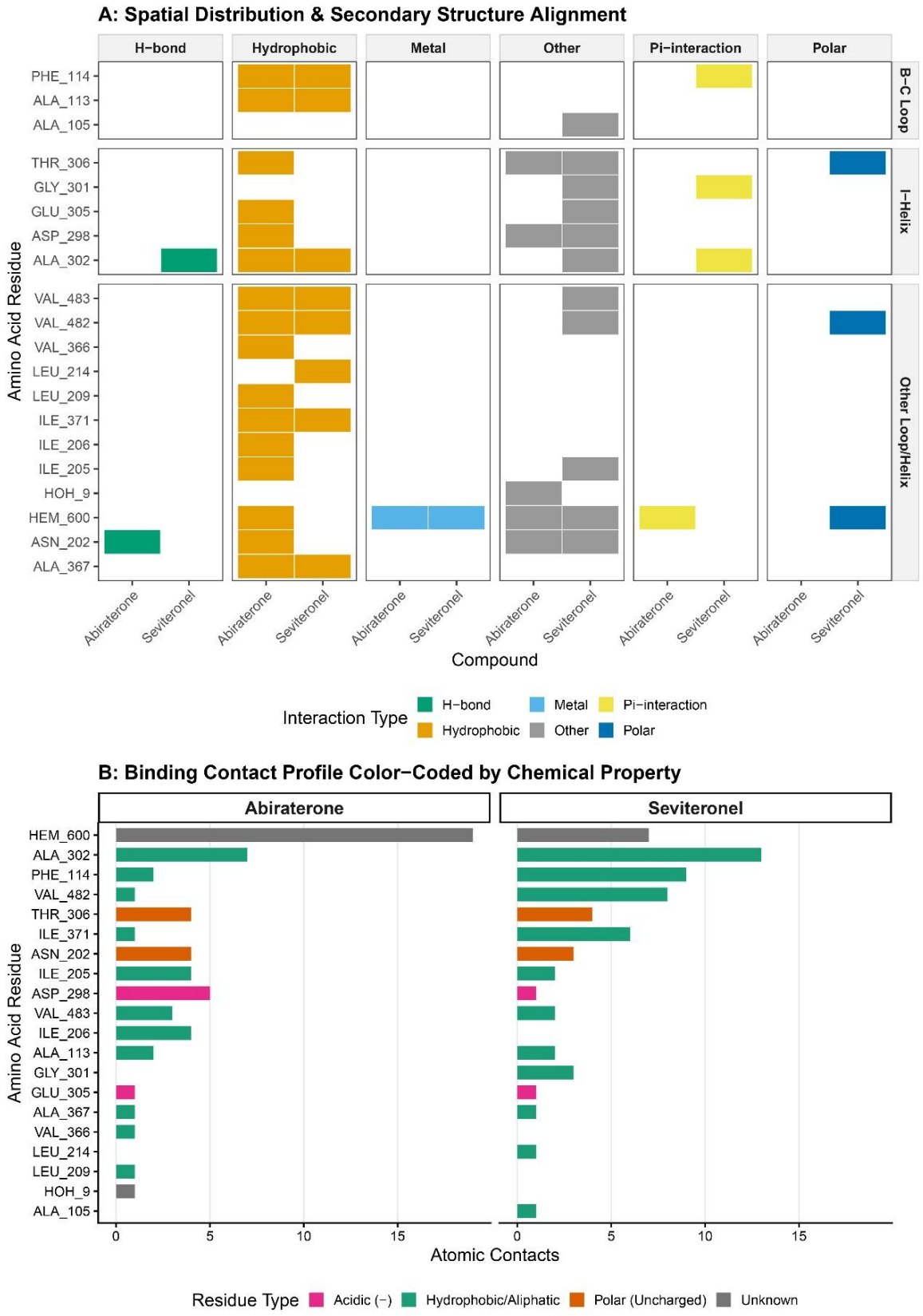

Figure S2. Residue-level interaction fingerprints of abiraterone and seviteronel within the CYP17A1 active site. (A) Spatial distribution of ligand–protein contacts according to interaction class and CYP17A1 structural region. Residues are grouped according to their location in the B–C-loop region, I-helix region, or

other active-site loops/helices. For each residue, contacts detected for abiraterone and seviteronel are classified as hydrogen-bonding, hydrophobic, metal-coordination, other van der Waals/close contacts, π-interactions, or polar interactions. The analysis highlights the distinct anchoring strategies of the two inhibitors: abiraterone combines heme coordination with the Asn202 hydrogen-bonding interaction and extensive hydrophobic packing, whereas seviteronel shows heme coordination together with contacts involving the I-helix and Val482-containing distal active-site region. HEM600 and HOH9 are included where ligand contacts with heme or crystallographic water were detected. **(B)** Residue-level contact profiles for abiraterone and seviteronel. Horizontal bars indicate the number of atom-level contacts assigned to each CYP17A1 residue or heme group in the structural interaction analysis. Bars are color-coded according to residue chemical class: acidic, hydrophobic/aliphatic, polar uncharged, or unclassified/non-amino-acid components. The contact count reflects the number of geometrically identified atom–atom interactions and should not be interpreted as an interaction-energy measurement. Together, the analyses illustrate concentrated steroid-core contacts for abiraterone and a different, more distributed contact pattern for seviteronel.

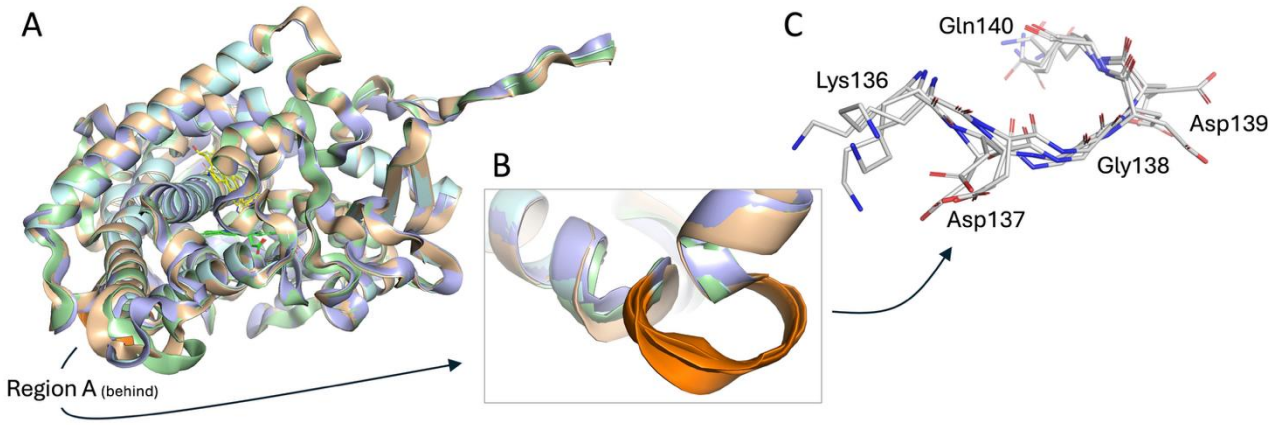

Figure S3. Structural comparison of CYP17A1 complexes in region A. Superposition of the CYP17A1 complexes with Abiraterone (3RUK_C and 3RUK_D), Orteronel (5IRQ_C) and Seviteronel (5IRV_C). Proteins are shown as cartoons and colored wheat, palegreen, lightblue and palecyan, respectively, except for the region A, which is colored orange. Heme and ligands are shown as sticks with C-atoms colored green and yellow, respectively, and heteroatoms colored by element. (**A**) Overall view. (**B**) Enlarged view of region A. (**C**) Superposition of residues Lys136, Asp137, Gly138, Asp139, and Gln140 within region A, illustrating ligand-associated differences in local backbone and side-chain geometry.

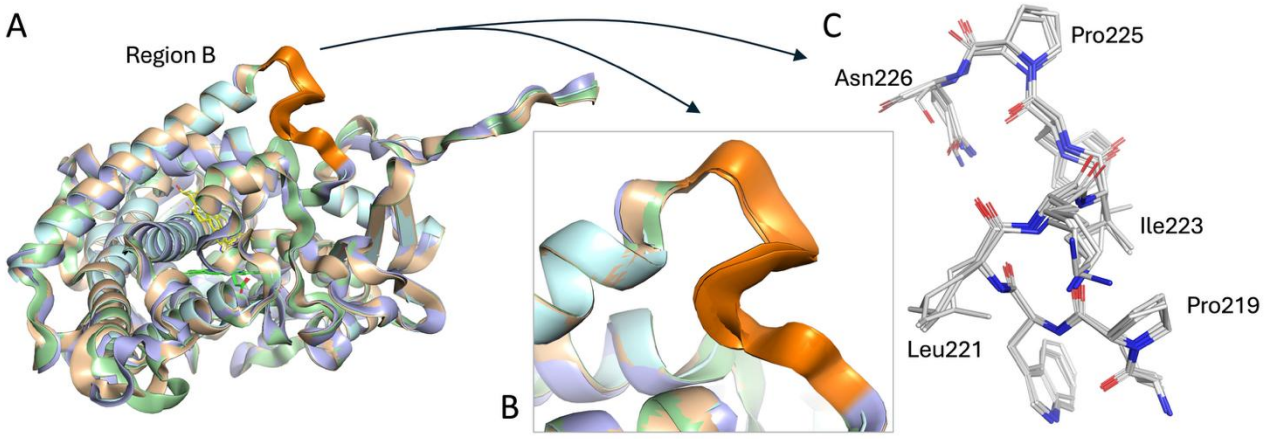

Figure S4. Structural comparison of CYP17A1 complexes in region B. Superposition of the CYP17A1 complexes with Abiraterone (3RUK_C and 3RUK_D), Orteronel (5IRQ_C) and Seviteronel (5IRV_C). Proteins are shown as cartoons and colored wheat, palegreen, lightblue and palecyan, respectively, except for the region B, which is colored orange. Heme and ligands are shown as sticks with C-atoms colored green and yellow, respectively, and heteroatoms colored by element. (A) Overall structural view showing the position of region B. (B) Enlarged superposition of region B. (C) Comparison of residues within this region, including Pro219, Leu221, Ile223, Pro225, and Asn226, showing local conformational differences among the four crystallographic models.

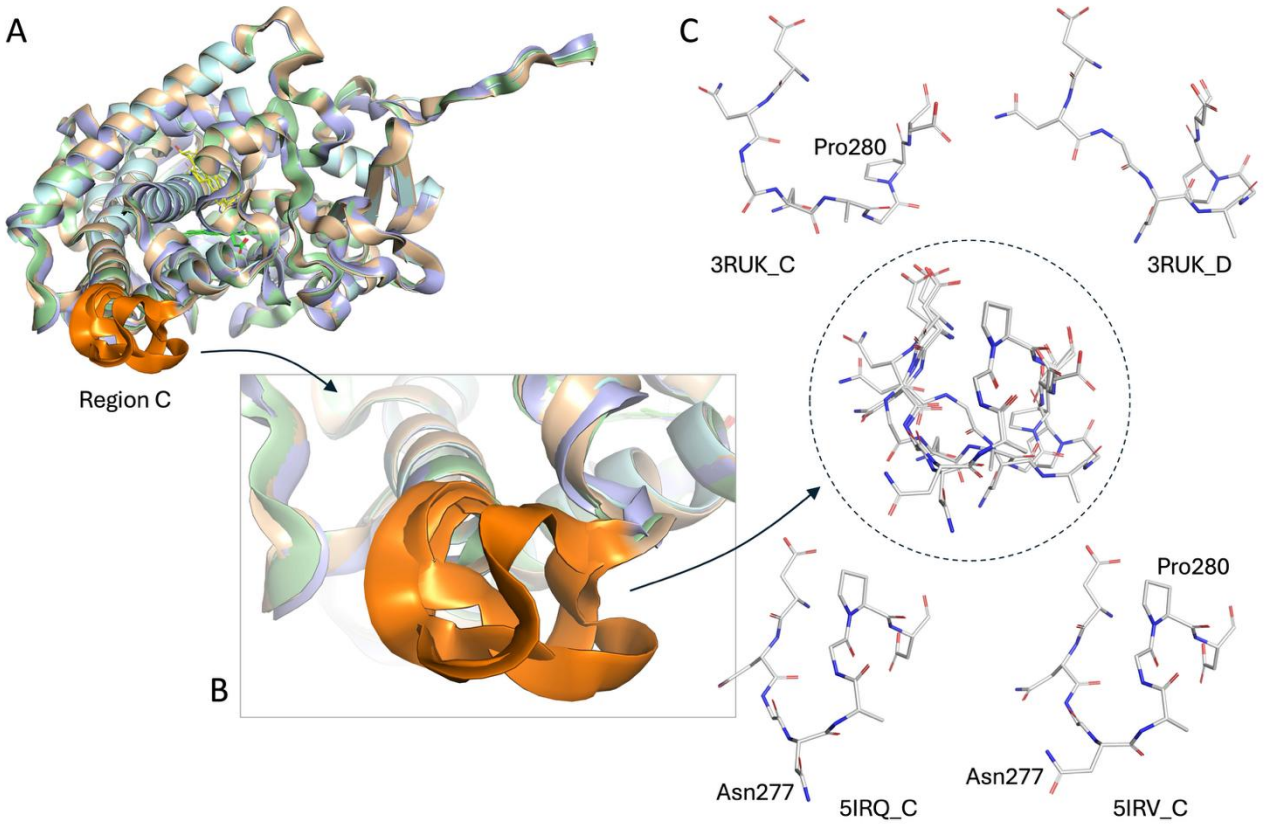

Figure S5. Structural comparison of CYP17A1 complexes in region C. Superposition of the CYP17A1 complexes with Abiraterone (3RUK_C and 3RUK_D), Orteronel (5IRQ_C) and Seviteronel (5IRV_C). Proteins are shown as cartoons and colored wheat, pale green, light blue and pale cyan, respectively, except for the region C, which is colored orange. Heme and ligands are shown as sticks with C-atoms colored green and yellow, respectively, and heteroatoms colored by element. (**A**) Overall structural view showing the position of region C. (**B**) Enlarged superposition of region C. (**C**) Local residue conformations shown both superposed and separately for the individual structures, highlighting differences around Asn277 and Pro280.

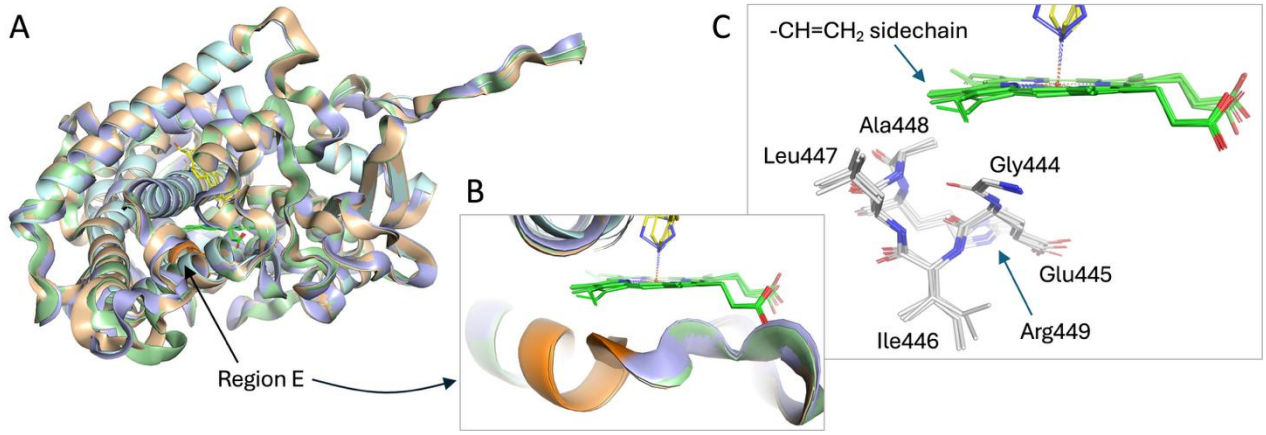

Figure S6. Structural comparison of CYP17A1 complexes in region E adjacent to the heme-binding region. Superposition of the CYP17A1 complexes with Abiraterone (3RUK_C and 3RUK_D), Orteronel (5IRQ_C) and Seviteronel (5IRV_C). Proteins are shown as cartoons and colored wheat, pale green, light blue and pale cyan, respectively, except for the region E, which is colored orange. Heme and ligands are shown as sticks with C-atoms colored green and yellow, respectively, and heteroatoms colored by element **(A)** Overall structural view showing the location of region E. **(B)** Enlarged view of region E in relation to the heme. **(C)** Superposition of residues Gly444, Glu445, Ile446, Leu447, Ala448, and Arg449 together with the heme group, illustrating local structural differences in the proximal heme-associated region.

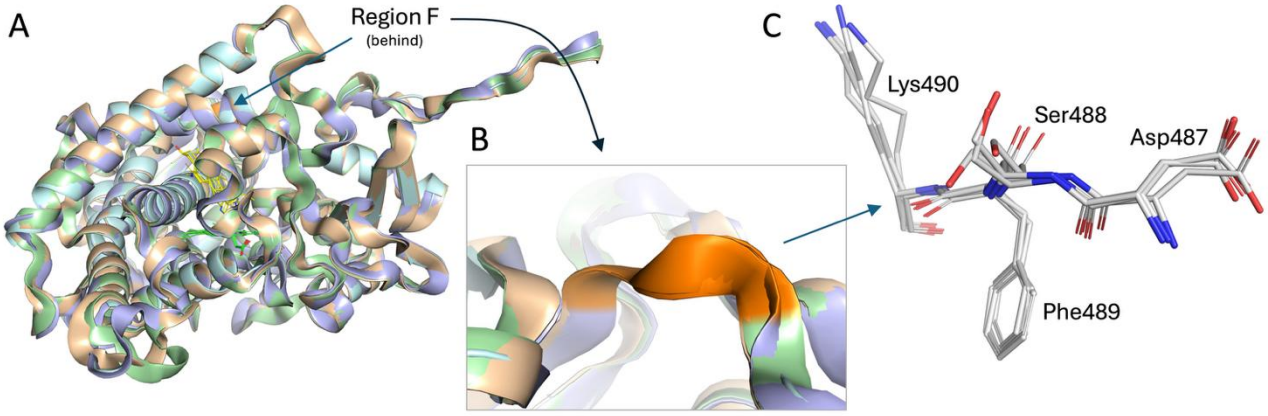

Figure S7: Structural comparison of CYP17A1 complexes in region F. Superposition of the CYP17A1 complexes with Abiraterone (3RUK_C and 3RUK_D), Orteronel (5IRQ_C) and Seviteronel (5IRV_C). Proteins are shown as cartoons and colored wheat, pale green, light blue and pale cyan, respectively, except for the region F, which is colored orange. Heme and ligands are shown as sticks with C-atoms colored green and yellow, respectively, and heteroatoms colored by element. (**A**) Overall view. (**B**) Zoom on region F. (**C**) Comparison of residues Asp487, Ser488, Phe489, and Lys490, highlighting local conformational differences among the inhibitor-bound structures.

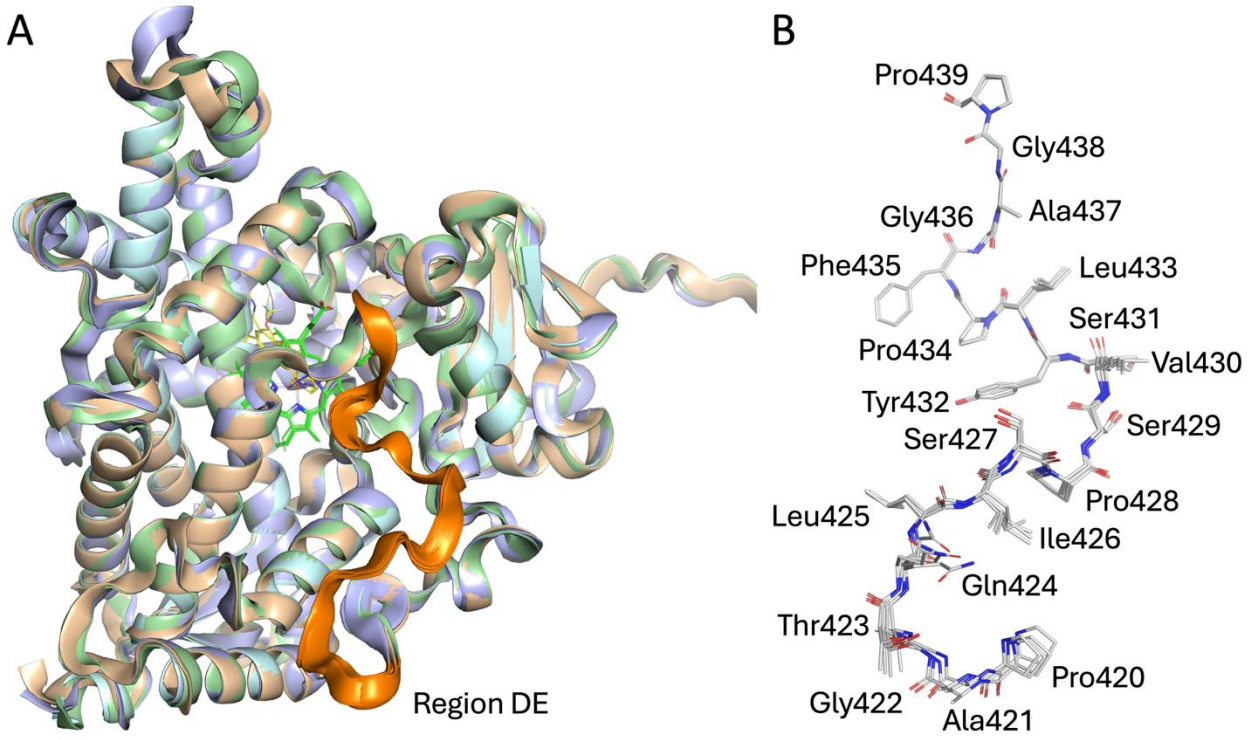

Figure S8. Structural comparison of CYP17A1 complexes in region DE. Superposition of abiraterone-bound CYP17A1 (3RUK_C and 3RUK_D), orteronel-bound CYP17A1 (5IRQ_C), and seviteronel-bound CYP17A1 (5IRV_C). Protein cartoons are colored wheat, pale green, light blue, and pale cyan, respectively; region DE is highlighted in orange. Heme and ligands are shown as sticks with carbon atoms colored green and yellow, respectively, and heteroatoms colored by element. (A) Overall structural view showing the position of region DE. (B) Superposition of residues spanning approximately Pro420–Pro439, including the intervening loop and secondary-structure elements. The panel illustrates local conformational differences among the starting inhibitor-bound CYP17A1 structures.

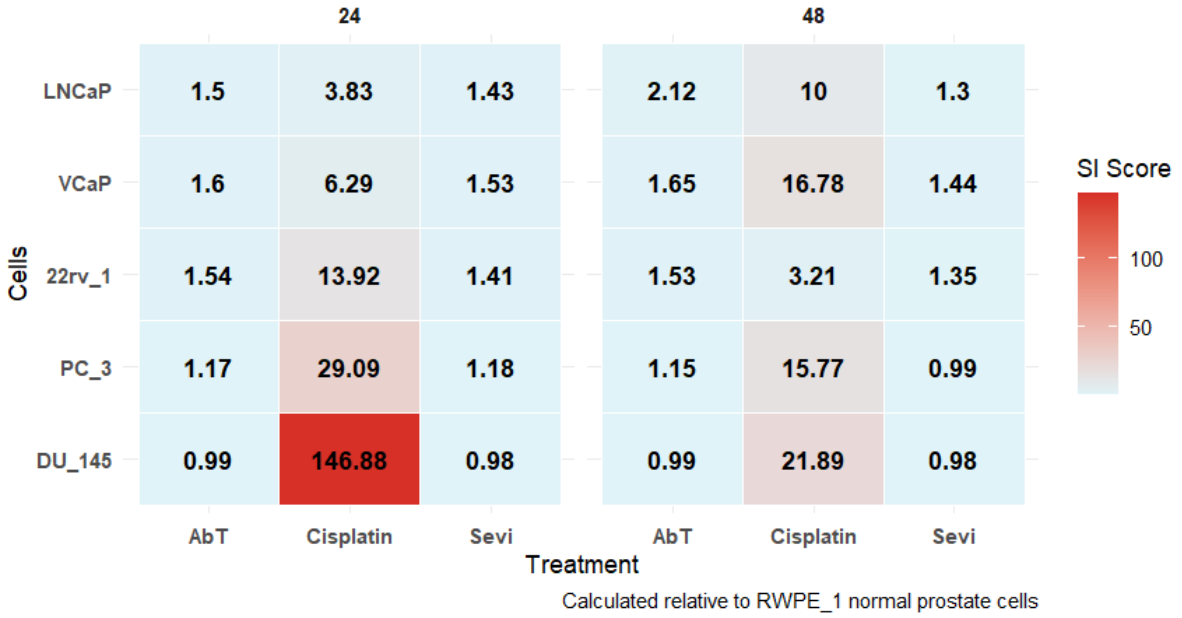

Figure S9. Relative treatment selectivity across prostate cancer cell lines. Heatmaps showing the relative selectivity ratio for abiraterone (AbT), seviteronel (Sevi), and cisplatin in LNCaP, VCaP, 22Rv1, PC-3, and DU-145 cells after 24 and 48 h of treatment. The ratio was calculated relative to the non-malignant prostate epithelial cell line RWPE-1 as: SI = viability of RWPE-1 cells / viability of the indicated cancer cell line under the same treatment and time point. Values >1 therefore indicate greater preservation of RWPE-1 viability relative to the corresponding cancer-cell line, whereas values close to or below 1 indicate little or no preferential effect on malignant cells. Values represent the same fixed-dose viability measurements summarized in Supplementary Table S4 and should not be interpreted as IC50-derived therapeutic indices.

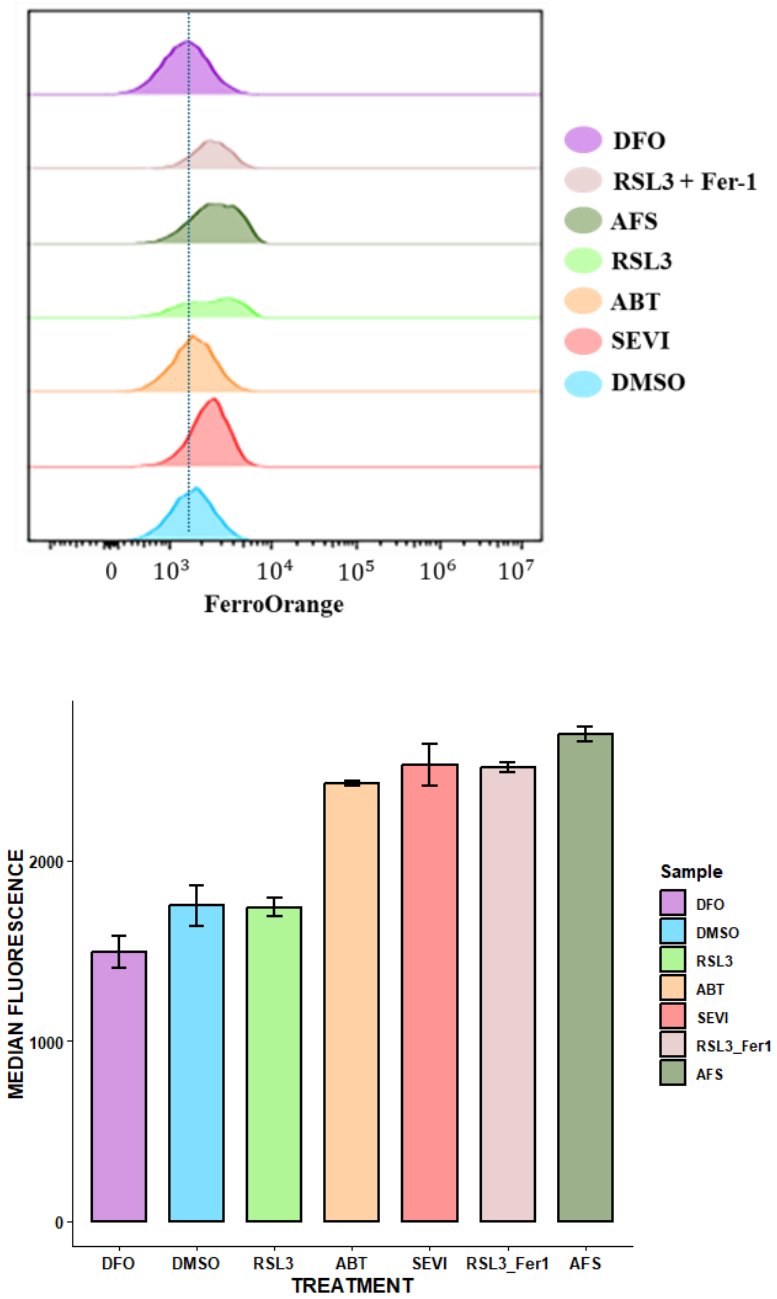

Figure S10. Quantification of the intracellular labile Fe^{2+} signal following treatment with abiraterone and seviteronel. Median FerroOrange fluorescence intensity was quantified in LNCaP cells treated with DMSO, Sevi, AbT, RSL3, RSL3 + ferrostatin-1 (Fer-1), and iron-loading conditions (AFS). DFO was included as an iron-chelation control. Fluorescence quantification confirmed that Sevi and AbT do not significantly increase intracellular labile Fe^{2+} levels, whereas iron-loading conditions enhanced FerroOrange fluorescence. Data are presented as mean ± SEM.

Supplementary Table S1: Primers for qPCR.

		Sequence orientation (5' - 3')	
Template	Primers	Forward	Reverse
NM_001382658.3	POR	CCGAGTTCACCAAAATTCAG	TCCCCGTTTTCTTCATCTTT
NM_002046.7	GAPDH	GCTCTCTGCTCCTCCTGTTC	CGACCAAATCCGTTGACTCC
NM_000102.4	CYP17A1	AACGTTGACTCCAGCATC	CCACTCCTTCTCATTGTGAT
NM_001190807.3	CYB5A	AAGGTGTACGATTTGACCAA	CGACATCCTCAAAGTTCTCA
NM_001166120.2	HSD3B2	CCACACCGCCTGTATCATTG	ACA CAGGCCTCCAACAGTAG
NM_003167.4	SULT2A1	GGTTTGACCACATTCATGGCTGG	CGGGTTCTAACGTCTTTCCCAG
NM_000781.3	CYP11A1	TGGCATCCTCTACAGACTCCTG	CTTCAGGTTGCGTGCCATCTCA
NM_001367832.1	GPX4	ACAAGAACGGCTGCGTGGTGAA	GCCACACACTTGTGGAGCTAGA
NM_014331.1	SLC7A11	TCCTGCTTTGGCTCCATGAACG	AGAGGAGTGTGCTTGCGGACAT
NM_203372.3	ACSL3	CTTTCTCACGGATGCCGCATTG	CTGCTGCCATCAGTGTTGGTTTC
NM_022977.3	ACSL4	GCTATCTCCTCAGACACACCGA	AGGTGCTCCAACTCTGCCAGTA
NM_001198696.2	AIFM2 (FSP1)	GACTCCTTCCACCACAATGTGG	CAGCACCATCTGGTTCTTCAGG
NM_001253908.2	AKR1C3	CCGAAGCAAGATTGCAGATGGC	GTGAGTTTTCCAAGGCTGGTCG
NM_001313966.2	TFRC	ATCGGTTGGTGCCACTGAATGG	ACAACAGTGGGCTGGCAGAAAC
NM_001145412.3	NFE2L2 (NRF2)	CACATCCAGTCAGAAACCAGTGG	GGAATGTCTGCGCCAAAAGCTG
NM_024111.6	CHAC1	GTGGTGACGCTCCTTGAAGATC	GAAGGTGACCTCCTTGGTATCG
NM_052839.4	PANX2	CCTCACCATCCTGAGCCGAAAC	GACGGTGCCATCCCTCAAAACT
NM_198291.3	SRC	CTGCTTTGGCGAGGTGTGGATG	CCACAGCATACAACTGCACCAG
NM_002394.6	SLC3A2	CCAGAAGGATGATGTCGCTCAG	GAGTAAGGTCCAGAATGACACGG

Supplementary Table S2. Quantitative steroid profiling of NCI-H295R cells following treatment with abiraterone (AbT), seviteronel (Sevi), or vehicle control (DMSO). Concentrations of pregnenolone, progesterone, 17α-hydroxyprogesterone, DHEA, and androstenedione are presented as mean ± SEM from independent experiments, together with calculated ratios reflecting CYP17A1 hydroxylase and 17,20-lyase activities.

	AbT		Sevi		DMSO	
nmol/L/mg of total protein	**Mean**	**SEM**	**Mean**	**SEM**	**Mean**	**SEM**
Cortisol	0.00230	0.00564	2.75790	0.37100	16.4927	0.88522
DHEA-S	0	0	3.91015	2.54006	33.0708	11.0934
Corticosterone	0	0	13.2202	0.65160	8.29302	2.11571
11-Deoxycortisol	31.9458	4.17166	68.0309	2.66722	394.932	48.7189
Androstendione	11.0401	0.86126	11.3567	1.195624	119.1583	13.33642
11-Deoxycorticosterone	5.572138	0.313269	271.3966	10.30716	151.6978	50.12917
Testosterone	0.576669	0.040399	0.464351	0.027734	1.462887	0.161141
DHEA	0.61422	0.34444	1.11060	0.45535	2.60832	0.72064
17α-Hydroxyprogesterone	1.668555	0.086578	28.13484	1.985571	11.95155	2.340863
Etiocholanolone	ND	ND	ND	ND	ND	ND
Progesterone	137.999	15.7190	65.0627	3.26977	2.11713	0.54419
Androsterone	ND	ND	ND	ND	ND	ND
Pregnenolone	222.641	24.5426	82.3308	3.89176	13.3095	4.63666
Aldosterone	0	0	0.27304	0.02944	0.16608	0.04195
Cortisone	0	0	0.123401	0.033817	0.388478	0.049691
21-Deoxycortisol	ND	ND	ND	ND	ND	ND
Dihydrotestosterone	ND	ND	ND	ND	ND	ND
11β-Hydroxyandrostenedione	0.473493	0.071504	5.254378	0.367968	1.184361	0.124302
6α-Hydroxyprogesterone	0.865814	0.060541	0.613534	0.111027	1.093606	0.077793
11β-hydroxy-5α-androstane-3,17-dione	0	0	16.35476	2.360823	0	0
16α-Hydroxyprogesterone	0.767878	0.138831	9.448073	1.578818	4.545525	0.247818
6β-Hydroxyprogesterone	1.706925	0.073813	0	0	1.541444	0.143841
5α-Pregnanetrione	0	0	22.47929	7.113791	37.12034	2.93294
17α-20α-Dihydroxyprogesterone	0	0	0.165171	0.049859	0.316149	0.075308
20α-OH Progesterone	0.358444	0.099948	0	0	0.846629	0.255226
20β-OH Progesterone	0.068788	0.029867	0	0	0	0
17α-OH Pregnenolone	0	0	19.93738	7.197524	93.78541	20.78369

Supplementary Table S3: Structural analysis of abiraterone and seviteronel binding to CYP17A1.

Feature	Abiraterone (PDB# 3RUK)	Seviteronel (VT-464, PDB# 5IRV)	Interpretation
Heme coordination	Pyridine nitrogen directly coordinates the heme Fe (≈2.0 Å).	Triazole nitrogen directly coordinates the heme Fe (≈2.2–2.3 Å).	Both inhibitors are classical type-II CYP17A1 ligands; iron coordination is conserved.
Scaffold	Steroidal tetracyclic androgen-like scaffold closely resembling endogenous CYP17A1 substrates.	Non-steroidal fused aromatic (naphthalene/aza-aromatic) scaffold bearing triazole and difluoromethoxy substituents.	Abiraterone exploits substrate mimicry, whereas seviteronel inhibits via a structurally distinct chemotype.
Primary polar interactions	3β-hydroxyl group forms a hydrogen bond with Asn202, with additional water-mediated stabilization reported in crystal structures.	the ligand hydroxyl oxygen O05 contacts the Val482 backbone carbonyl. (≈2.9 Å); no equivalent steroidal Asn202 hydroxyl anchor is present.	Abiraterone retains the canonical steroid-recognition hydrogen-bond network, whereas seviteronel relies on an alternative polar anchoring strategy.
Helix I / catalytic-region interactions	Steroid nucleus packs against Gly301, Ala302, and Thr306, producing extensive hydrophobic complementarity around the Helix I.	The triazole-containing moiety lies adjacent to Gly301, Ala302, and Thr306; a polar contact with Thr306 (≈3.0 Å) is observed in the interaction diagram.	Both ligands engage the catalytic Helix I region, but abiraterone does so through rigid steroid packing, whereas seviteronel positions a smaller heteroaromatic scaffold within the same region.
Additional polar contacts	Asn202 is the dominant direct hydrogen-bond partner; other nearby residues (e.g., Asp298/Glu305)	Interaction diagrams show close contacts involving Asn202, Asp298, and fluorine-containing substituents. These should be described as close electrostatic/van der	Fluorine contacts should be interpreted cautiously because organic fluorine rarely forms

	contribute weak or indirect contacts depending on refinement/model.	Waals or fluorine-mediated contacts rather than conventional hydrogen bonds.	strong classical hydrogen bonds in proteins.
Hydrophobic interaction	Ala113, Phe114, Ile205, Ile206, Leu209, Ala302, Thr306, Ala367, Ile371, Val482 and Val483 surround the steroid core.	Ala105, Ala113, Phe114, Ile205, Ile206, Arg239, Gly301, Ala302, Thr306, Ala367, Ile371, Val482 and Val483 contribute to the non-steroidal binding pocket.	Both inhibitors occupy essentially the same buried active site, but abiraterone forms a compact steroid-centered hydrophobic cluster, whereas seviteronel distributes contacts across its aromatic scaffold.
Orientation within the active site	Steroid nucleus extends toward the substrate-recognition region while maintaining a nearly vertical orientation above the heme.	Aromatic scaffold adopts a slightly different tilt, extending toward the Gly301/Ala302/Arg239 region while maintaining triazole–heme coordination.	Differences in ligand orientation alter the surrounding interaction network without changing the conserved heme ligation.
Functional differences	Potent inhibitor of both 17α-hydroxylase and 17,20-lyase activities with relatively limited catalytic selectivity.	Weaker absolute CYP17A1 potency but a higher lyase/hydroxylase selectivity index in the present assays using biochemical and cellular studies.	Differences in potency and selectivity.

Supplementary Table S4: Selectivity Index (SI) of treatments. Quantification of treatment specificity compared to RWPE_1 cells. SI > 1.0 indicates higher cytotoxicity towards malignant cells compared to normal epithelial cells.

Cell Line	Agent	24h Mean Viability (%)	24h Selectivity Index	48h Mean Viability (%)	48 h Selectivity Index
LNCaP	AbT	62.88	1.50	45.37	2.12
LNCaP	Cisplatin	12.01	3.83	3.85	10.00
LNCaP	Sevi	65.00	1.43	67.36	1.30
VCaP	AbT	59.19	1.60	58.11	1.65
VCaP	Cisplatin	7.30	6.29	2.29	16.78
VCaP	Sevi	60.66	1.53	60.92	1.44
22rv_1	AbT	61.24	1.54	62.88	1.53
22rv_1	Cisplatin	3.30	13.92	12.01	3.21
22rv_1	Sevi	65.89	1.41	65.00	1.35
PC_3	AbT	80.53	1.17	83.19	1.15
PC_3	Cisplatin	1.58	29.09	2.44	15.77
PC_3	Sevi	78.81	1.18	88.83	0.99
DU_145	AbT	95.12	0.99	96.57	0.99
DU_145	Cisplatin	0.31	146.88	1.76	21.89
DU_145	Sevi	94.25	0.98	89.84	0.98